Why reducing the cosmic sound horizon can not fully resolve the Hubble tension

Karsten Jedamzik
Laboratoire de Univers et Particules de Montpellier
Levon Pogosian
Simon Fraser University
Gong-Bo Zhao (gbzhao@nao.cas.cn)
National Astronomy Observatories, Chinese Academy of Sciences https://orcid.org/0000-0003-4726-6714

Letter

Keywords: Hubble tension, ΛCDM model, cosmic sound horizon

Posted Date: November 11th, 2020

DOI: https://doi.org/10.21203/rs.3.rs-100387/v1

Version of Record: A version of this preprint was published at Communications Physics on June 8th, 2021. See the published version at https://doi.org/10.1038/s42005-021-00628-x.

Why reducing the cosmic sound horizon can not fully resolve the Hubble tension

Karsten Jedamzik[1], Levon Pogosian[2], Gong-Bo Zhao[3,4]

The mismatch between the locally measured expansion rate of the universe and the one inferred from the cosmic microwave background measurements by Planck in the context of the standard ΛCDM, known as the Hubble tension, has become one of the most pressing problems in cosmology. A large number of amendments to the ΛCDM model have been proposed in order to solve this tension. Many of them introduce new physics, such as early dark energy, modifications of the standard model neutrino sector, extra radiation, primordial magnetic fields or varying fundamental constants, with the aim of reducing the sound horizon at recombination $r_\star$. We demonstrate here that any model which *only* reduces $r_\star$ can never fully resolve the Hubble tension while remaining consistent with other cosmological datasets. We show explicitly that models which operate at lower matter density $\Omega_m h^2$ run into tension with the observations of baryon acoustic oscillations, while models operating at higher $\Omega_m h^2$ develop tension with galaxy weak lensing data.

Decades of progress in observational and theoretical cosmology have led to the consensus that our universe is well described by a flat Friedman-Robertson-Lemaitre metric and is currently comprised of around 5% baryons, 25% cold dark matter (CDM), and 70% dark energy in its simplest form – the cosmological constant Λ. Although this ΛCDM model fits many observations exquisitely well, its prediction for the present day cosmic expansion rate, $H_0 = 67.36 \pm 0.54$ km/s/Mpc [1], based on precise cosmic microwave background (CMB) radiation observations by

the Planck satellite, do not compare well with direct measurements of the Hubble constant. In particular, the Supernovae H0 for the Equation of State (SH0ES) collaboration [2], using Cepheid calibrated supernovae Type Ia, finds a much higher value of $H_0 = 73.5 \pm 1.4$ km/s/Mpc. This 4.2σ disagreement, known as the "Hubble tension", has spurred much interest in modifications of the ΛCDM model capable of resolving it (cf. [3] for a comprehensive list of references). Several other determinations of H_0, using different methods, are also in some degree of tension with Planck, such as the Megamaser Cosmology Project [4] finding 73.9 ± 3.0 km/s/Mpc or H0LiCOW [5] finding $73.3^{+1.7}_{-1.8}$ km/s/Mpc. It is worth noting that a somewhat lower value of 69.8 ± 2.5 km/s/Mpc was obtained using an alternative method for calibrating SNIa [6].

Among the most precisely measured quantities in cosmology are the locations of the acoustic peaks in the CMB temperature and anisotropy spectra. They determine the angular size of the sound horizon at recombination,

$$\theta_\star \equiv \frac{r_\star}{D(z_\star)}, \tag{1}$$

with an accuracy of 0.03% [1]. The sound horizon $r_\star$ is the comoving distance a sound wave could travel from the beginning of the universe to recombination, a standard ruler in any given model, and $D(z_\star)$ is the comoving distance from a present day observer to the last scattering surface, *i.e.*, to the epoch of recombination. $D(z_\star)$ is determined by the redshift-dependent expansion rate $H(z) = h(z) \times 100$ km/s/Mpc which (see Sec. 1 in Methods for details), in a flat ΛCDM model, depends only on two parameters: $\Omega_m h^2$ and h, where Ω_m is the fractional matter energy density today and $h = h(0) = H_0/100$ km/s/Mpc. Thus, given $r_\star$ and an estimate of $\Omega_m h^2$, one can infer h from the measurement of $\theta_\star$ (see Sec. 1 in Methods for details). Planck anisotropy spectra provide

a constraint of $\Omega_m h^2 = 0.143 \pm 0.001$ within the ΛCDM model [1], yielding a Hubble constant significantly lower than the more direct local measurements.

If the value of the Hubble constant was the one measured locally, *i.e.*, $h \approx 0.735$, it would yield a much larger value of $\theta_\star$ unless something else in Eq. (1) was modified to preserve the observed CMB acoustic peak positions. There are two broad classes of models attempting to resolve this tension by introducing new physics. One introduces modifications at late times (*i.e.*, lower redshifts), *e.g.*, by introducing a dynamical dark energy or new interactions among the dark components that alter the Hubble expansion to make it approach a higher value today, while still preserving the integrated distance D in Eq. (1). In the second class of models, the new physics aims to reduce the numerator in Eq. (1), *i.e.*, modify the sound horizon at recombination.

Late time modifications based on simple phenomenological parameterizations tend to fall short of fully resolving the tension [8]. This is largely because the baryon acoustic oscillation (BAO) and and supernovae (SN) data, probing the expansion in the $0 \lesssim z \lesssim 1$ range, are generally consistent with a constant dark energy density. One can accommodate a higher value of H_0 by making parameterizations more flexible, as *e.g.*, in [9,10], that allow for a non-monotonically evolving effective dark energy fluid. Such non-monotonicity tends to imply instabilities within the context of simple dark energy and modified gravity theories [11] but can, in principle, be accommodated within the general Horndeski class of scalar-tensor theories [12].

Early-time solutions aim to reduce $r_\star$ with essentially two possibilities: (i) a coincidental increase of the Hubble expansion around recombination or (ii) new physics that alters the rate of

recombination. Proposals in class (i) include the presence of early dark energy [13–18], extra radiation in either neutrinos [19–22] or some other dark sector [23–28], and dark energy-dark matter interactions [29]. Proposals in class (ii) include primordial magnetic fields [30], non-standard recombination [31], or varying fundamental constants [32,33]. In this work we show that any early-time solution which only changes $r_\star$ can never fully resolve the Hubble tension without being in significant tension with either the weak lensing surveys [34,35] or BAO [36] observations.

The acoustic peaks, prominently seen in the CMB anisotropy spectra, are also seen as BAO peaks in the galaxy power spectra and carry the imprint of a slightly different, albeit intimately related, standard ruler – the sound horizon at the "cosmic drag" epoch (or the epoch of baryon decoupling), $r_{\rm d}$, when the photon drag on baryons becomes unimportant. As the latter takes place at a slightly lower redshift than recombination, we have $r_{\rm d} \approx 1.02 r_\star$ with the proportionality factor being essentially the same in all proposed modified recombination scenarios. More importantly for our discussion, the BAO feature corresponds to the angular size of the standard ruler at $z \ll z_\star$, *i.e.*, in the range $0 \lesssim z \lesssim 2.5$ accessible by galaxy redshift surveys. For the BAO feature measured using galaxy correlations in the transverse direction to the line of sight, the observable is

$$\theta^{\rm BAO}(z_{\rm obs}) \equiv \frac{r_{\rm d}}{D(z_{\rm obs})}\,, \tag{2}$$

where $z_{\rm obs}$ is the redshift at which a given BAO measurement is made. It is well known that BAO measurements at multiple redshifts provide a constraint on $r_{\rm d}h$ and $\Omega_{\rm m}$.

Without going into specific models, we now consider modifications of ΛCDM which decrease $r_\star$, treating the latter as a free parameter and taking $r_{\rm d} = 1.0184 r_\star$. For a given $\Omega_{\rm m}h^2$, Eq. (1)

defines a line in the $r_{\rm d}$-H_0 plane[1], and since Eqs. (1) and (2) are the same in essence, a BAO measurement at each different redshift also defines a respective line in the $r_{\rm d}$-H_0 plane. However, the significant difference between $z_\star$ and $z_{\rm obs}$ results in different slopes of the respective $r_{\rm d}(h)$ lines (see Sec. 1 in Methods for details), as illustrated in Fig. 1. The latter shows the $r_{\rm d}(h)$ lines from two different BAO observations, one at redshift $z = 0.5$ and another at $z = 1.5$, at $\Omega_{\rm m}h^2$ fixed to the Planck best fit ΛCDM value of 0.143, and the analogous lines defined by the CMB acoustic scale plotted for three values of $\Omega_{\rm m}h^2$: 0.143, 0.155 and 0.167. The lines are derived from the central observational values and do not account for the uncertainties in $\theta^{\rm BAO}$ and $\theta_\star$ (although the uncertainty in $\theta_\star$ is so tiny that it would be difficult to see by eye on this plot). As anticipated, the slope of the $r_{\rm d}(h)$ lines becomes steeper with increased redshift.

Also shown in Fig. 1 are the marginalized 68% and 95% confidence levels (CL) derived from the combination of all presently available BAO observations in a recombination-model-independent way (see [39] for details). The red contours show the ΛCDM based constraint from Planck, in good agreement with BAO at $H_0 \approx 67$ km/s/Mpc, but in tension with the SH0ES value shown with the grey band. In order to reconcile Planck with SH0ES solely by reducing $r_{\rm d}$, one would have to move along one of the CMB lines. Doing it along the line at $\Omega_{\rm m}h^2 = 0.143$ would quickly move the values of $r_{\rm d}$ and H_0 out of the purple band, creating a tension with BAO. Full consistency between the observed CMB peaks, BAO and the SH0ES Hubble constant could only be achieved at a higher value of $\Omega_{\rm m}h^2 \approx 0.167$. However, unless one supplements the reduction in $r_{\rm d}$ by yet another modification of the model, such high values of $\Omega_{\rm m}h^2$ would cause tension with galaxy weak

[1] In any specific model, $\Omega_{\rm m}h^2$ is well-constrained by CMB, but the best fit values vary.

lensing surveys such as the Dark Energy Survey (DES) [34] and the Kilo-Degree Survey (KiDS) [35], which we illustrate next.

DES and KiDS derived strong constraints on the quantity $S_8 \equiv \sigma_8(\Omega_m/0.3)^{0.5}$, where σ_8 is the matter clustering amplitude on the scale of $8\ h^{-1}$Mpc, as well as $\Omega_{\rm m}$. The value of S_8 depends on the amplitude and the spectral index of the spectrum of primordial fluctuations, which are well-determined by CMB and have similar best fit values in all modified recombination models. S_8 also depends on the net growth of matter perturbations which increases with more matter, *i.e.*, a larger $\Omega_{\rm m}h^2$.

The values of S_8 and $\Omega_{\rm m}$ obtained by DES and KiDS are already in slight tension with the Planck best fit ΛCDM model. Increasing the matter density aggravates this tension – a trend that can be seen in Fig. 2. The figure shows the 68% and 95% CL joint constraints on S_8-$\Omega_{\rm m}$ by DES, along with those by Planck within the ΛCDM model. The purple contours (Model 2) correspond to the model that can simultaneously fit BAO and CMB acoustic peaks at $\Omega_{\rm m}h^2 = 0.155$, *i.e.*, the model defined by the overlap between the BAO band and the $\theta_\star^{(2)}$ (blue dashed) line in Fig. 1. The green contours (Model 3) are derived from the model with $\Omega_{\rm m}h^2 = 0.167$ corresponding to the overlap region between the $\theta_\star^{(3)}$ (green dotted) line and the BAO and SH0ES bands in Fig. 1 (see Sec. 2 in Methods for details). The figure shows that when attempting to find a full resolution of the Hubble tension, with CMB, BAO and SH0ES in agreement with each other, one exacerbates the tension with DES and KiDS.

We note that there is much more information in the CMB than just the positions of the

acoustic peaks. It is generally not trivial to introduce new physics that reduces $r_\star$ and $r_{\rm d}$ without also worsening the fit to other features of the temperature and polarization spectra [41]. Our argument is that one will generally run into problems even before considering these additional potential complications.

Surveying the abundant literature of the proposed early-time solutions to the Hubble tension, one finds that the above trends are always confirmed. Fig. 3 shows the best fit values of $r_{\rm d}h$, H_0 and S_8 in models from Refs. [14,15,19,24,25,29–31,33]. One can see that, except for the model represented by the red dot at the very right of the plot, corresponding to the strongly interacting neutrino model of [19], solutions which operate at low $\Omega_{\rm m}h^2$ are in tension with BAO, whereas solutions operating at higher $\Omega_{\rm m}h^2$ are in tension with DES and KiDS. This tension was extensively discussed in the context of the early dark energy models [42–46]. As we have shown, it is part of a more general trend [2].

In most of the models represented in Fig. 3, the effect of introducing new physics only amounts to a reduction in $r_{\rm d}$. As we have argued, this will necessarily limit their ability to address the Hubble tension while staying consistent with the large scale structure data. Resolving the Hubble tension by new early-time physics without creating other observational tensions requires more than just a reduction of the sound horizon. This is exemplified by the interacting dark matter-dark radiation model [26] and the neutrino model [19] proposed as solutions. Here, extra tensions are avoided by supplementing the reduction in the sound horizon due to extra radiation by additional

[2]Note that there are other proposed early-time solutions to the Hubble tension. Fig. 3 only shows the models for which explicit estimates of H_0, $\Omega_m h^2$, S_8, and possibly $r_{\rm d}h$ were provided.

exotic physics: dark matter-dark radiation interactions in the first case and neutrino self-interactions and non-negligible neutrino masses in the second case. Consequently, with so many parameters, the posteriori probabilities for cosmological parameters are highly inflated over those for ΛCDM. It is not clear how theoretically appealing such scenarios are.

In conclusion, we have argued that any model which tries to reconcile the CMB inferred value of H_0 with that measured by SH0ES by only reducing the sound horizon automatically runs into tension with either the BAO or the galaxy weak lensing data. With just a reduction of $r_\star$, the highest value of the Hubble constants one can get, while remaining in a reasonable agreement with BAO and DES/KiDS, is around 70 km/s/Mpc. Thus, a full resolution of the Hubble tension will require either multiple modifications of the ΛCDM model or discovering systematic effects in one or more of the datasets.

1. Aghanim, N. et al. Planck 2018 results. VI. Cosmological parameters. Astron. Astrophys. **641**, A6 (2020).

2. Reid, M., Pesce, D. & Riess, A. An Improved Distance to NGC 4258 and its Implications for the Hubble Constant. Astrophys. J. Lett. **886**, L27 (2019).

3. Di Valentino, E. et al. Cosmology Intertwined II: The Hubble Constant Tension (2020). 2008.11284.

4. Pesce, D. et al. The Megamaser Cosmology Project. XIII. Combined Hubble constant constraints. Astrophys. J. **891**, L1 (2020).

5. Wong, K. C. et al. H0LiCOW XIII. A 2.4% measurement of H_0 from lensed quasars: 5.3σ tension between early and late-Universe probes (2019). 1907.04869.

6. Freedman, W. L. et al. The Carnegie-Chicago Hubble Program. VIII. An Independent Determination of the Hubble Constant Based on the Tip of the Red Giant Branch (2019). 1907.05922.

7. Ivanov, M. M., Ali-Haïmoud, Y. & Lesgourgues, J. H0 tension or T0 tension? Phys. Rev. D **102**, 063515 (2020).

8. Benevento, G., Hu, W. & Raveri, M. Can Late Dark Energy Transitions Raise the Hubble constant? Phys. Rev. D **101**, 103517 (2020).

9. Zhao, G.-B. et al. Dynamical dark energy in light of the latest observations. Nature Astron. **1**, 627–632 (2017).

10. Wang, Y., Pogosian, L., Zhao, G.-B. & Zucca, A. Evolution of dark energy reconstructed from the latest observations. Astrophys. J. Lett. **869**, L8 (2018).

11. Zucca, A., Pogosian, L., Silvestri, A., Wang, Y. & Zhao, G.-B. Generalized Brans-Dicke theories in light of evolving dark energy. Phys. Rev. D **101**, 043518 (2020).

12. Raveri, M. Reconstructing Gravity on Cosmological Scales. Phys. Rev. D **101**, 083524 (2020).

13. Karwal, T. & Kamionkowski, M. Dark energy at early times, the Hubble parameter, and the string axiverse. Phys. Rev. D **94**, 103523 (2016).

14. Poulin, V., Smith, T. L., Karwal, T. & Kamionkowski, M. Early Dark Energy Can Resolve The Hubble Tension. Phys. Rev. Lett. **122**, 221301 (2019).

15. Agrawal, P., Cyr-Racine, F.-Y., Pinner, D. & Randall, L. Rock 'n' Roll Solutions to the Hubble Tension (2019). 1904.01016.

16. Lin, M.-X., Benevento, G., Hu, W. & Raveri, M. Acoustic Dark Energy: Potential Conversion of the Hubble Tension (2019).

17. Berghaus, K. V. & Karwal, T. Thermal Friction as a Solution to the Hubble Tension. Phys. Rev. D **101**, 083537 (2020).

18. Niedermann, F. & Sloth, M. S. Resolving the Hubble Tension with New Early Dark Energy. Phys. Rev. D **102**, 063527 (2020).

19. Kreisch, C. D., Cyr-Racine, F.-Y. & Doré, O. Neutrino puzzle: Anomalies, interactions, and cosmological tensions. Phys. Rev. D **101**, 123505 (2020).

20. Sakstein, J. & Trodden, M. Early Dark Energy from Massive Neutrinos as a Natural Resolution of the Hubble Tension. Phys. Rev. Lett. **124**, 161301 (2020).

21. Archidiacono, M., Gariazzo, S., Giunti, C., Hannestad, S. & Tram, T. Sterile neutrino self-interactions: H_0 tension and short-baseline anomalies (2020). 2006.12885.

22. Escudero, M. & Witte, S. J. A CMB search for the neutrino mass mechanism and its relation to the Hubble tension. Eur. Phys. J. C **80**, 294 (2020).

23. Anchordoqui, L. A. & Perez Bergliaffa, S. E. Hot thermal universe endowed with massive dark vector fields and the Hubble tension. Phys. Rev. D **100**, 123525 (2019).

24. Gonzalez, M., Hertzberg, M. P. & Rompineve, F. Ultralight Scalar Decay and the Hubble Tension (2020). 2006.13959.

25. Pandey, K. L., Karwal, T. & Das, S. Alleviating the H_0 and σ_8 anomalies with a decaying dark matter model. JCAP **07**, 026 (2020).

26. Lesgourgues, J., Marques-Tavares, G. & Schmaltz, M. Evidence for dark matter interactions in cosmological precision data? JCAP **02**, 037 (2016).

27. Buen-Abad, M. A., Schmaltz, M., Lesgourgues, J. & Brinckmann, T. Interacting Dark Sector and Precision Cosmology. JCAP **01**, 008 (2018).

28. Kumar, S., Nunes, R. C. & Yadav, S. K. Cosmological bounds on dark matter-photon coupling. Phys. Rev. D **98**, 043521 (2018).

29. Agrawal, P., Obied, G. & Vafa, C. H_0 Tension, Swampland Conjectures and the Epoch of Fading Dark Matter (2019). 1906.08261.

30. Jedamzik, K. & Pogosian, L. Relieving the Hubble tension with primordial magnetic fields (2020). 2004.09487.

31. Chiang, C.-T. & Slosar, A. Inferences of H_0 in presence of a non-standard recombination (2018). 1811.03624.

32. Hart, L. & Chluba, J. Updated fundamental constant constraints from Planck 2018 data and possible relations to the Hubble tension. Mon. Not. Roy. Astron. Soc. **493**, 3255–3263 (2020).

33. Sekiguchi, T. & Takahashi, T. Early recombination as a solution to the H_0 tension (2020). 2007.03381.

34. Abbott, T. M. C. et al. Dark Energy Survey year 1 results: Cosmological constraints from galaxy clustering and weak lensing. Phys. Rev. **D98**, 043526 (2018).

35. Asgari, M. et al. KiDS-1000 Cosmology: Cosmic shear constraints and comparison between two point statistics (2020). 2007.15633.

36. Alam, S. et al. The clustering of galaxies in the completed SDSS-III Baryon Oscillation Spectroscopic Survey: cosmological analysis of the DR12 galaxy sample. Mon. Not. Roy. Astron. Soc. **470**, 2617–2652 (2017).

37. Eisenstein, D. J. et al. Detection of the Baryon Acoustic Peak in the Large-Scale Correlation Function of SDSS Luminous Red Galaxies. Astrophys. J. **633**, 560–574 (2005).

38. du Mas des Bourboux, H. et al. The Completed SDSS-IV extended Baryon Oscillation Spectroscopic Survey: Baryon acoustic oscillations with Lyman-α forests (2020).

39. Pogosian, L., Zhao, G.-B. & Jedamzik, K. Recombination-independent determination of the sound horizon and the Hubble constant from BAO (2020).

40. Joudaki, S. et al. KiDS+VIKING-450 and DES-Y1 combined: Cosmology with cosmic shear. Astron. Astrophys. **638**, L1 (2020).

41. Knox, L. & Millea, M. Hubble constant hunter's guide. Phys. Rev. D **101**, 043533 (2020).

42. Hill, J. C., McDonough, E., Toomey, M. W. & Alexander, S. Early dark energy does not restore cosmological concordance. Phys. Rev. D **102**, 043507 (2020).

43. Ivanov, M. M. et al. Constraining Early Dark Energy with Large-Scale Structure (2020). 2006.11235.

44. D'Amico, G., Senatore, L., Zhang, P. & Zheng, H. The Hubble Tension in Light of the Full-Shape Analysis of Large-Scale Structure Data (2020). 2006.12420.

45. Murgia, R., Abellán, G. F. & Poulin, V. The early dark energy resolution to the Hubble tension in light of weak lensing surveys and lensing anomalies (2020). 2009.10733.

46. Smith, T. L. et al. Early dark energy is not excluded by current large-scale structure data (2020). 2009.10740.

47. Lewis, A. & Bridle, S. Cosmological parameters from CMB and other data: A Monte Carlo approach. Phys. Rev. D **66**, 103511 (2002).

48. Lewis, A. GetDist: a Python package for analysing Monte Carlo samples (2019). URL https://getdist.readthedocs.io. 1910.13970.

Correspondence Correspondence and requests for materials should be addressed to G. B. Zhao (email: gbzhao@nao.cas.cn).

Acknowledgements We thank Eiichiro Komatsu and Joulien Lesgourgues for helpful comments on the draft of the paper and Kanhaiya Pandy and Toyokazu Sekiguchi for kindly providing us with data of their models. We gratefully acknowledge using `CosmoMC` [47] and `GetDist` [48]. This research was enabled in part by support provided by WestGrid (`www.westgrid.ca`) and Compute Canada Calcul Canada (`www.computecanada.ca`). L.P. is supported in part by the National Sciences and Engineering Research Council (NSERC) of Canada, and by the Chinese Academy of Sciences President's International Fellowship Initiative, Grant No. 2020VMA0020. G.B.Z. is supported by the National Key Basic Research and Development Program of China (No. 2018YFA0404503), a grant of CAS Interdisciplinary Innovation Team, and NSFC Grants 11925303, 11720101004, 11673025 and 11890691.

Author contributions K.J. proposed the idea, drafted the manuscript and participated in all stages of the project; L.P. co-developed the idea, ran the numerical simulations and contributed to the text; G-B. Z. developed the numerical code used in this work, and contributed to the text.

Author Information [1]*Laboratoire de Univers et Particules de Montpellier, UMR5299-CNRS, Universite de Montpellier, 34095 Montpellier, France*

[2]*Department of Physics, Simon Fraser University, Burnaby, British Columbia, Canada V5A 1S6*

[3]*National Astronomy Observatories, Chinese Academy of Science, Beijing, 100101, P.R.China*

[4]*University of Chinese Academy of Sciences, Beijing, 100049, P.R.China*

Competing Interests The authors declare that they have no competing financial interests.

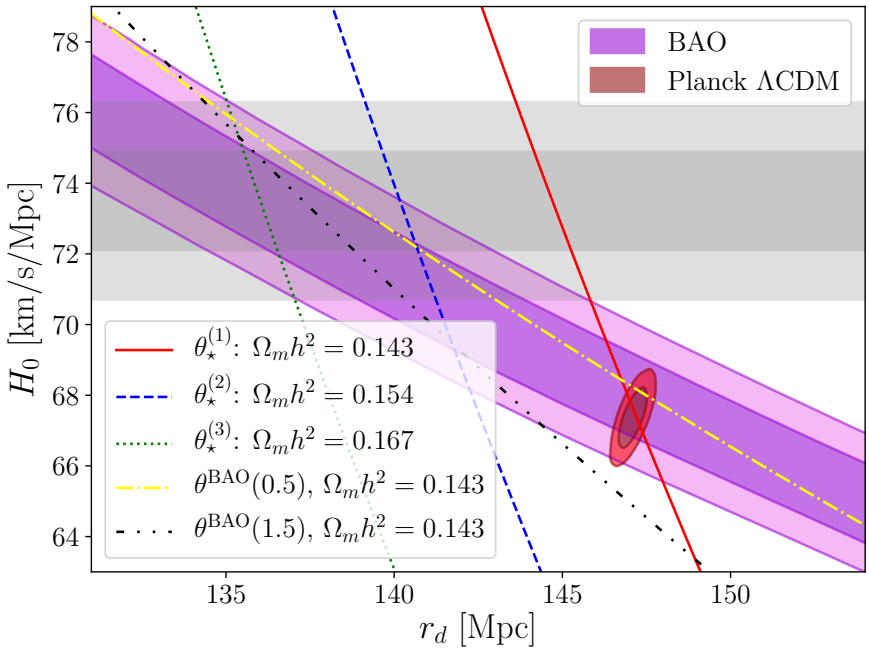

Figure 1. A plot illustrating that achieving a full agreement between CMB, BAO and SH0ES through a reduction of $r_{\rm d}$ requires a higher value of $\Omega_{\rm m}h^2$.

Shown are the lines of degeneracy between the sound horizon $r_{\rm d}$ and the Hubble constant H_0 defined by the CMB acoustic scale $\theta_\star$ at three different values of $\Omega_{\rm m}h^2$: 0.143, 0.155 and 0.167. Also shown are the marginalized 68% and 95% CL bands derived from the combination of all current BAO data, and the ΛCDM based bounds from Planck. To demonstrate how the slope of the lines changes with redshift, we show two lines corresponding to the SDSS measurements of $\theta^{\rm BAO}$ at $z = 0.51$ and $z = 1.5$ [38] at a fixed $\Omega_{\rm m}h^2 = 0.143$. The grey band shows the 68% and 95% CL determination of the Hubble constant by SH0ES.

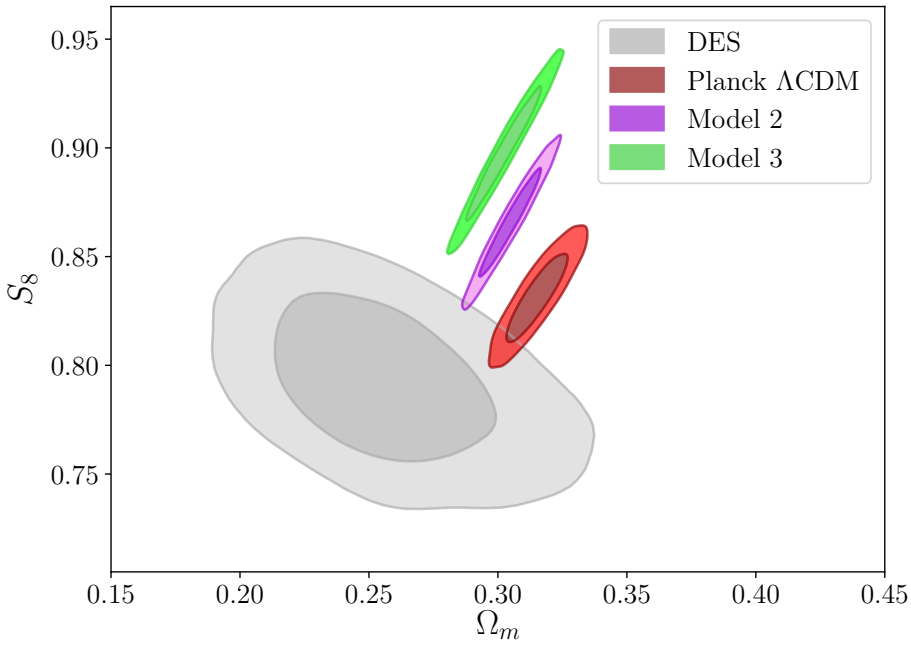

Figure 2. The 68% and 95% CL bounds on S_8 and $\Omega_{\rm m}$ from DES, along with those in the Planck best fit ΛCDM model and two other models.

Model 2 is defined by the simultaneous fit to BAO and CMB acoustic peaks at $\Omega_{\rm m}h^2 = 0.155$, *i.e.*, the overlap between the BAO band and the $\theta_\star^{(2)}$ line in Fig. 1. Model 3 has $\Omega_{\rm m}h^2 = 0.167$ and corresponds to the overlap region between the $\theta_\star^{(3)}$ line and the BAO and SH0ES bands in Figure 1.

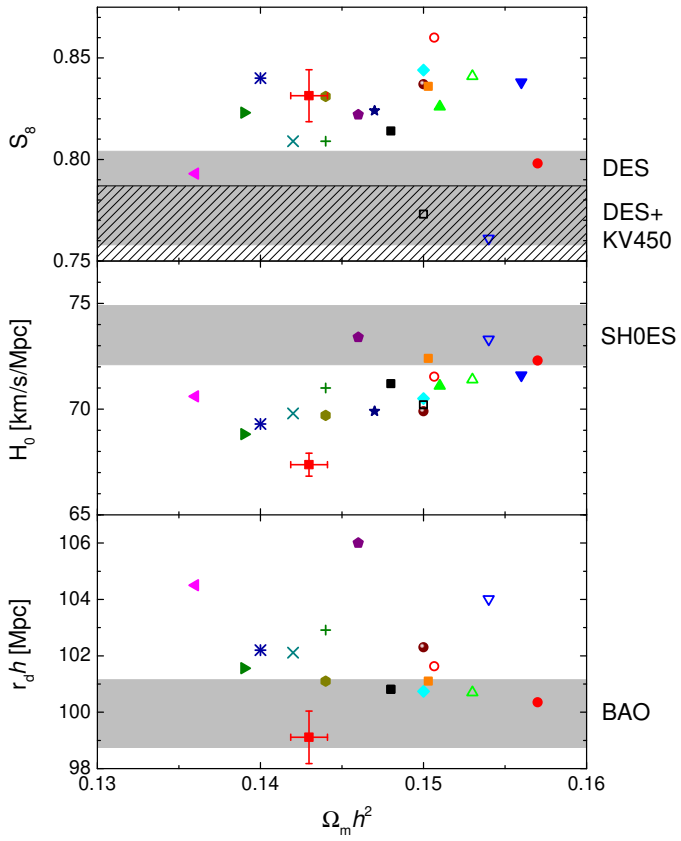

Figure 3. A compilation of values of $r_{\rm d}h$, H_0 and S_8 predicted by the models in Refs. [14,15,15,19,24,25,29–31,33], along with the 68% CL bands from BAO [39], SH0ES, DES [34] and the combination of DES with KiDS (KV450) [40].

The correspondence between each symbol and theoretical model with references is shown in Supplementary Figure 1, and the red square point with error bars represents the Planck best fit ΛCDM model [1]. With the exception of the red dot, corresponding to the model from [19] with multiple modifications of ΛCDM, there is a consistent trend: models with low $\Omega_{\rm m}h^2$ either fail to achieve a sufficiently high H_0 or are in tension with BAO, and models with high values of $\Omega_{\rm m}h^2$ run into tension with DES/KiDS.

Methods

1 The acoustic scale measurements from the CMB and BAO

The geometric information of the Universe is mapped by the CMB via

$$\theta_\star \equiv \frac{r_\star}{D(z_\star)} = \frac{\int_{z_\star}^{\infty} c_s(z)\mathrm{d}z/H(z)}{\int_0^{z_\star} c\,\mathrm{d}z/H(z)}\,, \tag{3}$$

where $z_\star \approx 1090$ is the redshift of cosmological recombination, $c_s(z)$ is the sound speed of the photon-baryon fluid, c is the speed of light, and $H(z)$ is the redshift-dependent cosmological expansion rate. The sound horizon $r_\star$ is the comoving distance a sound wave could travel from the beginning of the universe to recombination, a standard ruler in any given model, and $D(z_\star)$ is the comoving distance from a present day observer to the last scattering surface, *i.e.*, to the epoch of recombination.

The redshift dependence of the Hubble parameter in the ΛCDM model can be written as

$$h(z) = \sqrt{\Omega_r h^2(1+z)^4 + \Omega_m h^2(1+z)^3 + \Omega_\Lambda h^2} \tag{4}$$

where $h(z)$ is simply $H(z)$ in units of 100 km/s/Mpc, and h is the value at redshift $z = 0$. Here, Ω_r, Ω_m and Ω_Λ are the present day density fractions of radiation, matter (baryons and CDM) and dark energy. From the precise measurement of the present-day CMB temperature $T_0 = 2.7255\,\mathrm{K}$ (however, also see [7]), and adopting the standard models of particle physics and cosmology, one knows the density of photons and neutrinos $\Omega_r h^2$. Using the theoretically well motivated criticality condition on the sum of the fractional densities, *i.e.*, $\Omega_r + \Omega_m + \Omega_\Lambda = 1$, one finds that $h(z)$ is dependent only on two remaining quantities: $\Omega_m h^2$ and h. The photon-baryon sound speed c_s in

Eq. (1) is determined by the ratio of the baryon and photon densities and is well-constrained by both Big Bang nucleosynthesis and the CMB. Thus, given an estimate of $\Omega_m h^2$, one can infer h from the measurement of $\theta_\star$.

There are three types of BAO observables corresponding to the three ways of extracting the acoustic scale from galaxy surveys [37]: using correlations in the direction perpendicular to the line of sight, using correlations in the direction parallel to the line of sight, and the angle-averaged or "isotropic" measurement. For the purpose of our discussion, it suffices to consider just the first type, which is the closest to CMB in its essence, but our conclusions apply to all three. In fact, our numerical analysis includes all three types. Namely, let us consider

$$\theta^{\rm BAO}(z_{\rm obs}) \equiv \frac{r_{\rm d}}{D(z_{\rm obs})} = \frac{\int_{z_{\rm d}}^{\infty} c_s(z){\rm d}z/H(z)}{\int_0^{z_{\rm obs}} c\,{\rm d}z/H(z)}\,, \tag{5}$$

where $z_{\rm obs}$ is the redshift at which a given BAO measurement is made.

As the integrals in the denominators of Eqs. (3) and (5) are dominated by the matter density at low redshifts, one can safely neglect $\Omega_r h^2$ and write

$$r_\star = \theta_\star \int_0^{z_\star} \frac{2998\,{\rm Mpc}\,{\rm d}z}{\omega_m^{1/2}\sqrt{(1+z)^3 + h^2/\omega_m - 1}}, \tag{6}$$

where $\omega_{\rm m} = \Omega_{\rm m} h^2$, and an analogous equation for BAO with the replacement $(r_\star, \theta_\star, z_\star) \to (r_{\rm d}, \theta^{\rm BAO}, z_{\rm obs})$. For a given $\Omega_{\rm m} h^2$, Eq. (6) defines a line in the $r_{\rm d}$-H_0 plane. Similarly, a BAO measurement at each different redshift also defines a respective line in the $r_{\rm d}$-H_0 plane. Taking the derivative of $r_\star$ with respect to h one finds

$$\frac{\partial r_\star}{\partial h} = -\frac{h}{\omega_m}\theta_\star \int_0^{z_\star} \frac{2998\,{\rm Mpc}\,{\rm d}z}{\omega_m^{1/2}\big((1+z)^3 + h^2/\omega_m - 1\big)^{3/2}} \tag{7}$$

and a completely analogous equation for BAO. It is important to realize that the derivative is very different for CMB and BAO due to the vast difference in redshifts at which the standard ruler is observed, $z_\star \approx 1100$ for CMB *vs* $z_{\rm obs} \sim 1$ for BAO, resulting in different values of the integral in Eq. (7). This results in different slopes of the respective $r_{\rm d}(h)$ lines.

2 Obtaining the S_8 constraints

To derive the Model 2 and Model 3 contours in Fig. 2, we fit the ΛCDM model to the BAO data using $r_{\rm d}$, $\Omega_{\rm m}h^2$ and h as a free parameters, supplemented by Gaussian priors on $\Omega_{\rm m}h^2$ and h, and with the primordial spectrum amplitude A_s and the spectral index n_s fixed to their best fit ΛCDM values. The fit then generates constraints on S_8 and $\Omega_{\rm m}$ as derived parameters. For Model 2, the Gaussian priors were $\Omega_{\rm m}h^2 = 0.155 \pm 0.0012$, where we assumed the same relative uncertainty in $\Omega_{\rm m}h^2$ as for the Planck best fit ΛCDM model, and $h = 0.71 \pm 0.01$, corresponding to the central value and the 1σ overlap between the CMB2 line and the BAO band. For Model 3, the priors were $\Omega_{\rm m}h^2 = 0.167 \pm 0.0013$ and $h = 0.735 \pm 0.14$.

Data Availability The data that support the plots within this paper and other findings of this study are available from the corresponding author upon reasonable request.

Supplementary Information

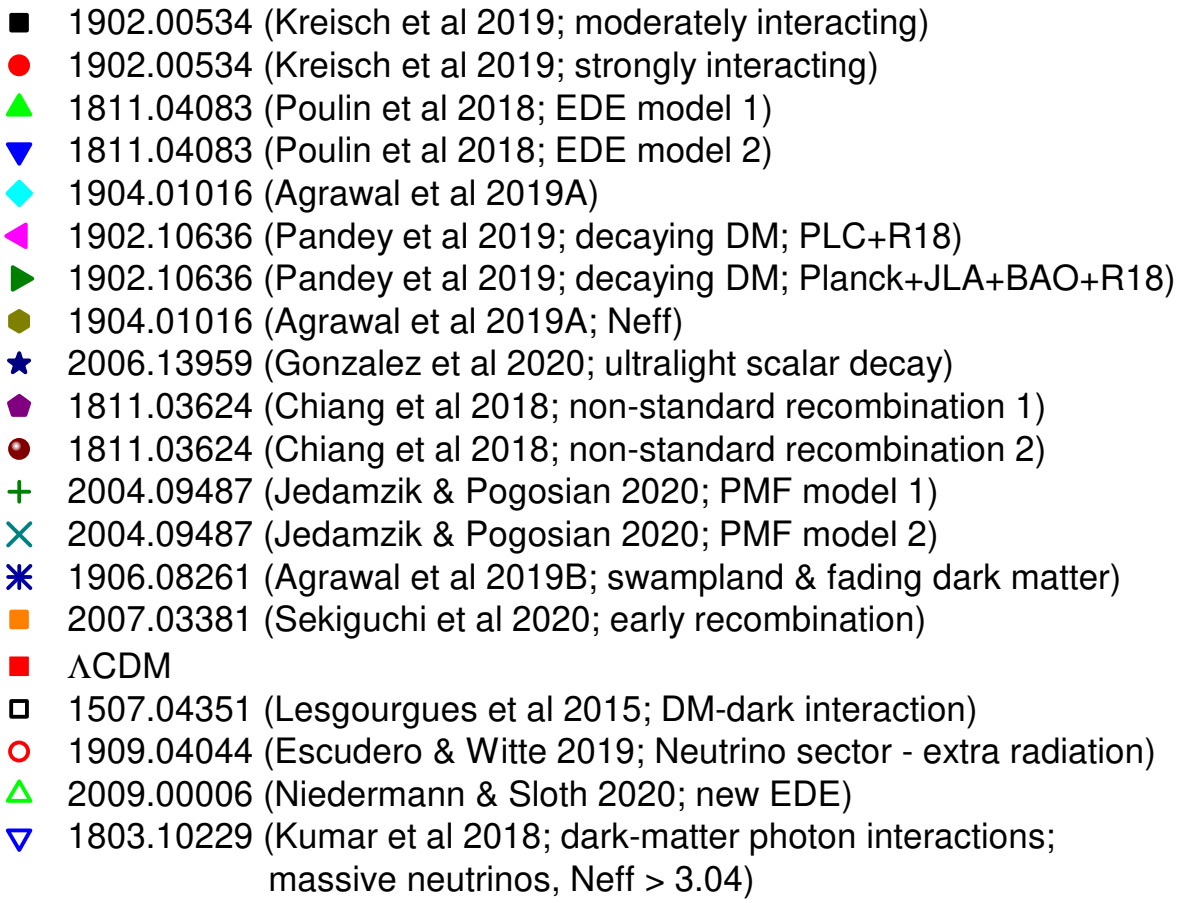

Supplementary Figure 1. The correspondence of symbols in Fig. 3 to theoretical models studied in the literature.

For each symbol, the arXiv number of the corresponding paper is listed, followed by a short description of the model shown in the parentheses.

Figures

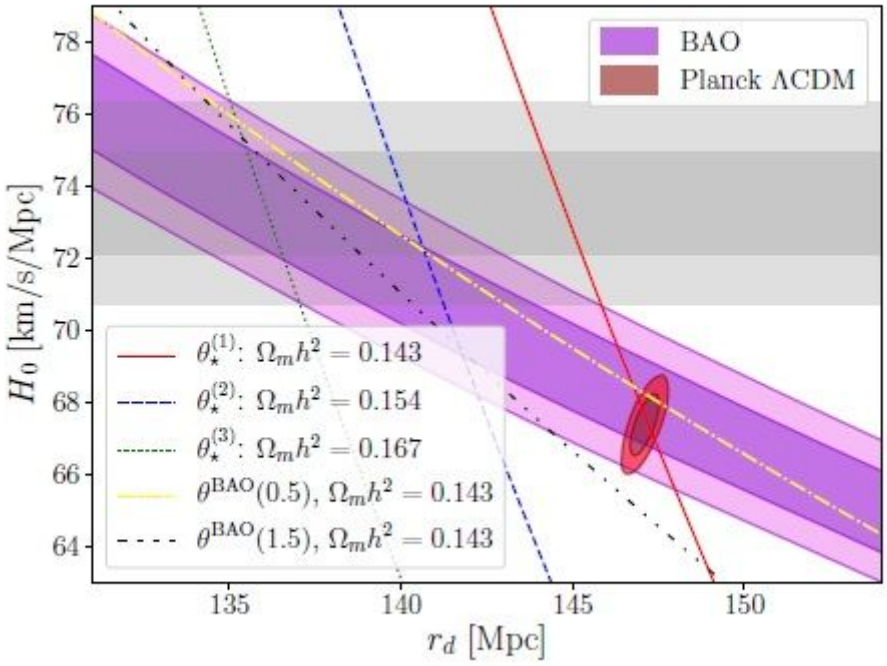

Figure 1

A plot illustrating that achieving a full agreement between CMB, BAO and SH0ES through a reduction of rd requires a higher value of mh2. Shown are the lines of degeneracy between the sound horizon rd and the Hubble constant H0 defined by the CMB acoustic scale? at three different values of mh2: 0:143, 0:155 and 0:167. Also shown are the marginalized 68% and 95% CL bands derived from the combination of all current BAO data, and the CDM based bounds from Planck. To demonstrate how the slope of the lines changes with redshift, we show two lines corresponding to the SDSS measurements of BAO at z = 0:51 and z = 1:5 38 at a fixed mh2 = 0:143. The grey band shows the 68% and 95% CL determination of the Hubble constant by SH0ES.

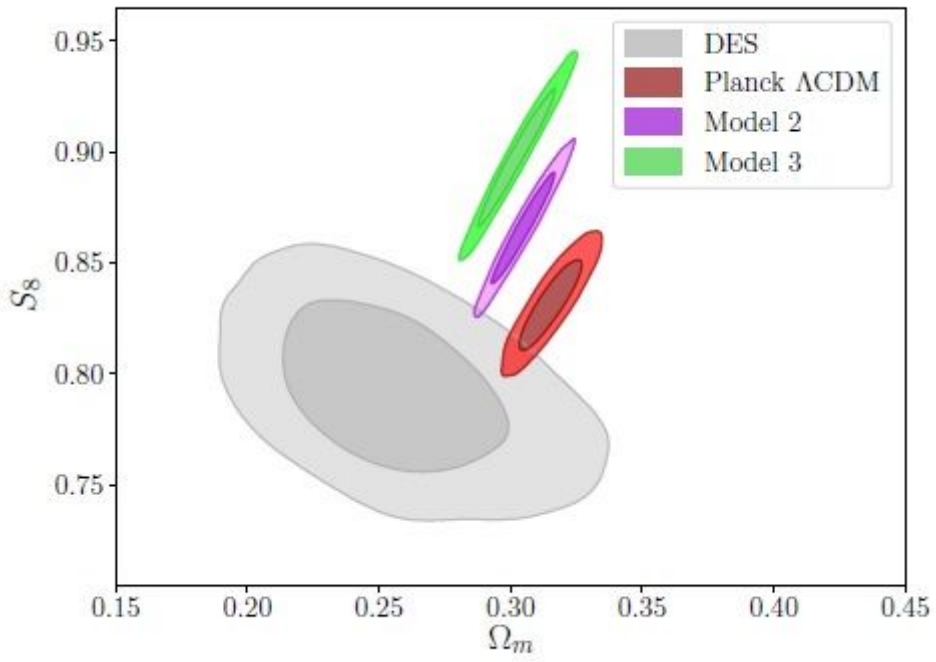

Figure 2

The 68% and 95% CL bounds on S8 and m from DES, along with those in the Planck best fit CDM model and two other models. Model 2 is defined by the simultaneous fit to BAO and CMB acoustic peaks at mh2 = 0:155, i.e., the overlap between the BAO band and the (2) ? line in Fig. 1. Model 3 has mh2 = 0:167 and corresponds to the overlap region between the (3) ? line and the BAO and SH0ES bands in Figure 1.

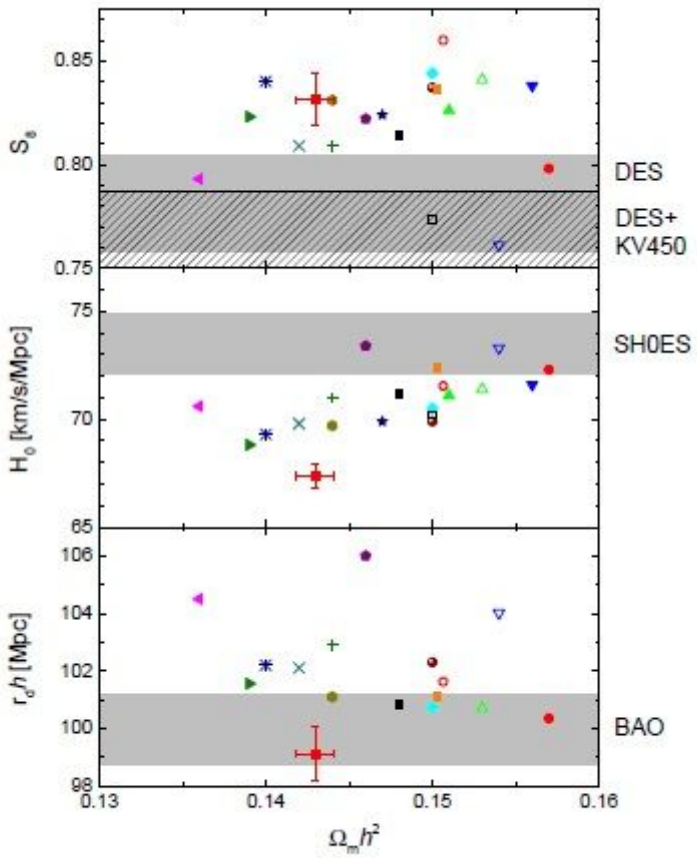

Figure 3

A compilation of values of rdh,H0 and S8 predicted by the models in Refs. 14, 15, 15, 19, 24, 25, 29–31, 33, along with the 68% CL bands from BAO 39, SH0ES, DES 34 and the combination of DES with KiDS (KV450) 40. The correspondence between each symbol and theoretical model with references is shown in Supplementary Figure 1, and the red square point with error bars represents the Planck best fit CDM model 1. With the exception of the red dot, corresponding to the model from 19 with multiple modifications of CDM, there is a consistent trend: models with low mh2 either fail to achieve a sufficiently high H0 or are in tension with BAO, and models with high values of mh2 run into tension with DES/KiDS.